Structure and NLO Properties of Layered Bimetallic Oxalato-Bridged Ferromagnetic Networks Containing Stilbazolium-Shaped Chromophores

S. Bénard,[†] P. Yu,[†] J. P. Audière,[†] E. Rivière,[†] R. Clément,*[,†] J. Guilhem,[‡] L. Tchertanov,*[,‡] and K. Nakatani[§]

Contribution from the Laboratoire de Chimie Inorganique, UMR 8613, Bt 420, Université Paris Sud, 91405 Orsay, France, the Laboratoire de Cristallochimie, Institut de Chimie des Substances Naturelles, UPR 2301, 91198 Gif-sur-Yvette, France and the P.P.S.M., Ecole Normale Supérieure de Cachan, URA 1906, avenue du Président Wilson, 94235 Cachan, France

Received January 24, 2000

Abstract: A series of 35 layered compounds $A[M^{II}Cr^{III}(C_2O_4)_3]\cdot n$ solvent has been synthesized with five different metals (M = Mn, Fe, Co, Ni, Cu) and seven hyperpolarizable stilbazolium-shaped A chromophores: (4-[4-(dimethylamino)-α-styryl]-N-alkylpyridinium), alkyl = methyl, ethyl, isopropyl (DAMS, DAES, DAPS respectively); (4-[4-methoxy-α-styryl]-N-alkylpyridinium), alkyl = isopentyl, heptyl (MIPS, MHS); DAZOP and CINDAMS are DAMS analogues, where the central [C=C] core has replaced by azo or butadiene cores, respectively)]. These compounds have been designed as possible multiproperty materials associating ferromagnetism and second-order optical nonlinearity. Two-third of these compounds exhibit second harmonic generation (with efficiency up to 100 times that of urea at 1.9 μm), the others being inactive. All of them order ferromagnetically below Curie temperatures that range from 6 to 13 K. The structures of DAPS[$Mn^{II}Cr^{III}(C_2O_4)_3$].$CH_3CN$ and MIPS[$Mn^{II}Cr^{III}(C_2O_4)_3$] have been resolved. Both of them belong to the centrosymmetric $P2_1/c$ space group, which accounts for their NLO inactivity. The long axes of the chromophores in a given layer are parallel, but the dipolar moments are antiparallel. Two successive chromophore layers along the stacking direction have approximately orthogonal orientations, giving rise to a doubling of the **c** parameter. X-ray powder diffraction shows that the high crystalline compounds of the series possess the same monoclinic unit cell as $A[Mn^{II}Cr^{III}(C_2O_4)_3]$ (A = DAPS, MIPS). A search for structure−property correlation emphasizes the relationship between a short interlayer distance and the alignment of the chromophore dipoles.

Introduction

There has been a tremendous activity over the past two decades in the areas of molecular-based magnets and of organic materials for quadratic nonlinear optics (NLO).[1−6] Both areas have now reached a considerable extent, but so far there has been virtually no overlap between them. The design of molecular multi-property materials that would possess both a strong NLO efficiency and a strong spontaneous magnetization below a reasonably high critical temperature still constitutes a challenge that deserves interest, as its achievement would allow studying the physics of such materials and determine whether unusual features arise from the coexistence of the two properties. A strategy based on intercalation chemistry had led in 1994 to an NLO active magnet $Mn_{1-x}PS_3(DAMS)_{2x}$, where DAMS stands for the stilbazolium-type chromophore defined in Scheme 1.[7−9] In this layered intercalation compound, the inorganic $MnPS_3$ host lattice acquires a spontaneous magnetization below about 35 K, and the inserted organic DAMS chromophores spontaneously pack in a non-centrosymmetrical way, forming extended *J*-type aggregates which bring about a large hyperpolarizability.[7] However, despite its interest, this material possesses a rather weak magnetization; hence, there is still a need for developing other families of compounds that would display stronger magnetization.

Among the two-dimensional hybrid organic−inorganic compounds encountered in the area of molecule-based magnets, the bimetallic trioxalatometalates $A[M^{II}M^{III}(ox)_3]$, where A stands for a monovalent organic cation, form a class of insulating compounds which are of interest due to their ferro- or ferrimagnetic properties at low temperature.[10−18] In these com-

[†] Laboratoire de Chimie Inorganique, University Paris-Sud.

[‡] Laboratoire de Cristallochimie, Institut de Chimie des Substances Naturelles of Gif-sur-Yvette.

[§] P.P.S.M., Ecole Normale Supérieure de Cachan.

(1) Kahn, O. *Molecular Magnetism*; VCH Publisher: New York, 1993.
(2) Miller, J. S.; Epstein, A. J. *Angew. Chem., Int. Ed. Engl.* **1994**, *33*, 385; *Chem. Eng. News* **1996**, *73(40)*, 30.
(3) Ferlay, S.; Mallah, T.; Ouahès, R.; Veillet, P.; Verdaguer, M. *Nature* **1995**, *378*, 701.
(4) Williams, D. J. *Angew. Chem., Int. Ed. Engl.* **1984**, *23*, 690.
(5) Zyss, J.; Ledoux, I.; Nicoud, J. F. In *Molecular Non-Linear Optics*; Zyss, J., Ed.; Academic Press: Boston 1993.
(6) Marder, S. R. In *Inorganic Materials*, 2nd ed.; Bruce, D. W., O'Hare, D., Eds.; John Wiley: Chichester, 1996; p 122.
(7) Lacroix, P. G.; Clément, R.; Nakatani, K.; Zyss, J.; Ledoux, I. *Science* **1994**, *263*, 658. Coradin, T.; Clément, R.; Lacroix, P. G.; Nakatani, K. *Chem. Mater.* **1996**, *8*, 2153.
(8) Clément, R.; Lacroix, P.; Evans, J. S. O.; O'Hare, D. *Adv. Mater.* **1994**, *6*, 794.
(9) Marder, S. R.; Perry, J. W.; Schaeffer, W. P. *Science* **1989**, *245*, 626.
(10) Tamaki, H.; Mitsumi, M.; Nakamura, K.; Matsumoto, N.; Kida, S.; Okawa, H.; Iijima, S. *Chem. Lett.* **1992**, 1975.
(11) Tamaki, H.; Zhong, Z. J.; Matsumoto, N.; Kida, S.; Koikawa, M.; Achiva, N.; Hashimoto, Y.; Okawa, H. *J. Am. Chem. Soc.* **1992**, *114*, 6974.
(12) Atovmyan, L. O.; Shilov, G. V.; Lyubovskaya, R. N.; Zhilyaeva, E. I.; Morozov, Y. G. *JETP Lett.* **1993**, *10*, 766.

10.1021/ja0002619 CCC: $19.00
Published on Web 09/13/2000

Scheme 1. Seven Cationic Chromophores Used in This Work

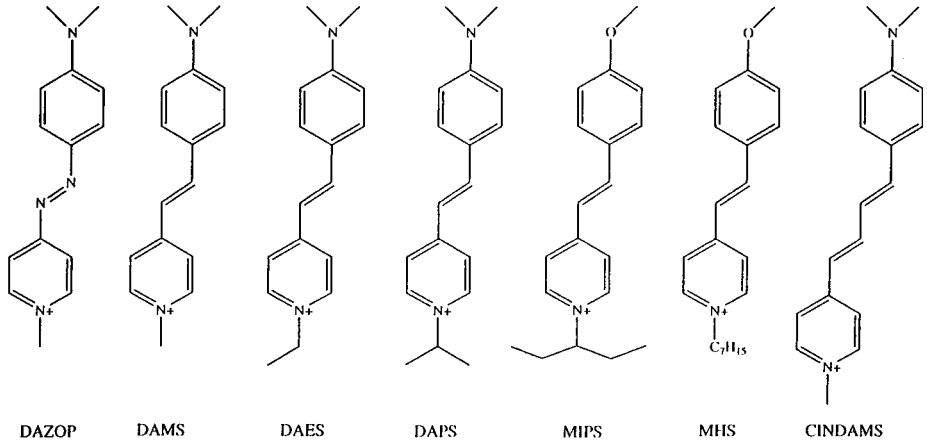

pounds, each inorganic slab is made up of divalent M^{II} ions held together by $[M^{III}(ox)_3]^{3-}$ units (M^{III} = Fe, Cr, Ru) that play the role of bridging ligands, in such a way that the M^{II} and M^{III} ions generate a honeycomb lattice. These inorganic slabs are separated by layers of organic cations, usually bulky ammonium or phosphonium $[XR_4]^+$ (X = N, P; R = Ph, Pr^n, Bu^n, Pn^n) species. A possible strategy to confer second-order NLO properties to these materials is to replace these "innocent" organic cations by hyperpolarizable species, under synthetic conditions where they will pack in a noncentrosymmetrical way.

Some of us have shown in 1997 that the crystallization of several layered trioxalatochromates with the methoxy heptyl stilbazolium cation (MHS, see Scheme 1) afforded hybrid compounds $MHS[M^{II}Cr(ox)_3]$, which were either strongly NLO active (M^{II} = Mn, Fe) or completely inactive (M^{II} = Co, Cu).[19] The formation of a similar compound with the DAMS chromophore has been also reported, but no NLO properties were described.[20] Following these preliminary results, we have undertaken a more general study aiming at crystallizing layered $A[M^{II}Cr^{III}(ox)_3]$ trioxalatochromates incorporating various chromophores belonging to the stilbazolium structural type. Our goal is not only to prepare new strongly NLO active magnets, but also to obtain structural information about the compounds in order to find out the factors governing the packing of the chromophores and hence the NLO activity.

Experimental Section

Synthesis of the Chromophore Salts. The cationic stilbazolium-shaped chromophores shown in Scheme 1 were synthesized by condensation of the 4-N-substituted picolinium iodide (or bromide) with the appropriate aldhehyde in ethanol by heating at reflux overnight in the presence of a catalytic amount of piperidine.[21−25] To increase the solubility of the ionic compounds obtained, the halide ions were replaced by nitrate ions by addition of silver nitrate to a solution of the halide in methanol and subsequent filtration of the precipitated silver halide. DAMS was used as the chloride and was prepared by exchanging I^- for Cl^- with a solution of AgCl in MeOH. MIPS was employed as the bromide. All the chromophore salts were identified by their ^1H NMR spectra (Bruker 250 MHz apparatus).

[DAZOP]I was synthesized by a two-step process, starting with the formation at ∼−15 °C of the diazo derivative of 4-aminopyridine in an acidic (2:1 phosphoric acid 85%/nitric acid 65%) solution of sodium nitrite. This solution was then slowly added to *N*,*N*-dimethylaniline in a buffer solution containing sodium carbonate. The resulting azo compound was then extracted with dichloromethane. An orange precipitate was obtained after complete evaporation of the solvent and addition of water. The 4-*N*-methylated iodide salt was obtained by overnight reflux in dichloromethane with a large excess of methyl iodide, then turned into chloride.[24]

Synthesis of the $A[M^{II}Cr(ox)_3]$ Compounds (M^{II} = Mn, Fe, Co, Ni, Cu). Thirty-five $A[M^{II}Cr(ox)_3]$ compounds (ox = C_2O_4) were obtained by combining five metallic ions (M^{II} = Mn, Fe, Co, Ni, Cu) with the seven chromophores shown in Scheme 1. These compounds were synthesized according to one of the following procedures.

Method 1. In a typical preparation, 0.2 mmol of the chromophore nitrate and 0.2 mmol of $[K_3Cr(ox)_3]3H_2O$ were dissolved in a mixture of 4 mL of methanol and 4 mL of water. When a precipitate formed at this stage, the solution was heated to 60 °C until redissolution. $M^{II}(NO_3)_2$ (0.2 mmol), dissolved in the minimum amount of methanol, was then added to the former solution. A precipitate appeared after a lapse of time, depending on the nature of the chromophore and of the metallic salt. The solid was then filtered out and successively washed with a mixture of water−methanol, then water, and finally methanol. The whole process was carried out under a nitrogen atmosphere in the case where M^{II} = Fe.

Method 2. A different procedure was designed for the DAZOP compounds. Aqueous solutions of [DAZOP]Cl and of $[K_3Cr(ox)_3]\cdot 3H_2O$ were mixed in a 3:1 molar ratio to precipitate $[DAZOP]_3[Cr(ox)_3]$. The latter was dissolved in a (1:1) mixture of methanol and acetonitrile, and subsequent addition of an equimolar amount of Mn^{II} or Co^{II} nitrate to this solution resulted in the rapid formation of a solid, which was then filtered and washed as above. When M^{II} = Fe, Ni, Cu, the addition of a small amount of water to the methanol/acetonitrile mixture turned out to improve considerably the crystallinity of the final compounds.

Elemental analyses of the compounds were obtained from the CNRS facility. Data are given in Table 1 for a panel of representative

(13) Decurtins, S.; Schmalle, H. W.; Oswald, H. R.; Linden, A.; Ensling, J.; Gütlich, P.; Hauser, A. *Inorg. Chim. Acta* **1994**, *216*, 65.
(14) Mathonière, C.; Carling, S. G.; Dou, Y.; Day, P. *J. Chem.* Soc., *Chem. Commun.* **1994**, 1551; Mathonière, C.; Nuttal, C. J.; Carling, S. G.; Day, P. *Inorg. Chem.* **1996**, *35*, 1201.
(15) Clemente-Leon, M.; Coronado, E.; Galan-Mascaros, J. R.; Gomez-Garcia, C. J. *J. Chem.* Soc., *Chem. Commun.* **1997**, 1727.
(16) Atovman, L. O.; Shilov, G. V.; Lyubovskaya, R. N.; Zhilyaeva, E. I.; Ovanesyan, N. S.; Bogdanova, O. A.; Perumova, S. I. *Russ. J. Coord. Chem.* **1997**, *23*, 640.
(17) Shilov, G. V.; Atovman, L. O.; Ovanesyan, N. S.; Pyalling, A. A.; Bottyan, L. *Russ. J. Coord. Chem.* **1998**, *24*, 288.
(18) Shilov, G. V.; Ovanesyan, N. S.; Sanina, N. A.; Pyalling, A. A.; Atovman, L. O. *Russ. J. Coord. Chem.* **1998**, *24*, 802.
(19) Bénard, S.; Yu, P.; Coradin, T.; Rivière, E.; Nakatani, K.; Clément, R. *Adv. Mater.* **1997**, *9*, 981.
(20) Gu, Z.; Sato, O.; Iyoda, T.; Hashimoto, K.; Fujishima, A. *Mol. Cryst. Liq. Cryst.* **1996**, *286*, 147.
(21) Kuo, K. T. *J. Chin. Chem. Soc.* **1978**, *25*, 131.
(22) Marder, S. R.; Perry, J. W.; Yakymyshyn, C. P. *Chem. Mater.* **1994**, *6*, 1137.
(23) Marder, S. R.; Perry, J. W.; Tiemann, B. G.; Marsh, R. E.; Schaeffer, W. P. *Chem. Mater.* **1990**, *2*, 685.
(24) Li, H.; Zhou, D.; Huang, C.; Xu, J.; Li, T.; Zhao, X.; Xia, X. *J. Chem. Soc., Faraday Trans.* **1996**, *92*, 2585.
(25) Matsui, M.; Kawamura, S.; Shibata, K.; Muramatsu, H. *Bull. Chem. Soc. Jpn.* **1992**, *65*, 71.

Table 1. Analytical and TGA Data of Selected A[MCr(ox)$_3$]·*n* Solv

	C% found(calcd)	H% found(calcd)	N% found(calcd)	M% found(calcd)	Cr% found(calcd)	TGA
DAMS[MnCr(ox)$_3$]	43.85 (43.29)	3.37 (3.14)	4.61 (4.59)	8.59 (9.00)	8.31 (8.52)	no solvent
DAMS[FeCr(ox)$_3$]	42.98 (43.23)	3.32 (3.13)	4.73 (4.58)	9.02 (9.14)	8.13 (8.51)	no solvent
DAMS[CuCr(ox)$_3$]·0.5MeOH	42.53 (42.56)	3.23 (3.33)	4.76 (4.41)	9.89 (10.01)	7.82 (8.19)	0.35 MeOH
DAZOP[MnCr(ox)$_3$]·0.5MeCN	39.58 (39.28)	2.91 (2.97)	10.06 (10.06)	8.28 (8.76)	7.69 (8.30)	0.47 MeCN
DAZOP[CoCr(ox)$_3$]	38.98 (38.96)	2.82 (2.78)	9.09 (9.09)	8.31 (8.43)	9.38 (9.57)	no solvent
DAZOP[NiCr(ox)$_3$]·MeCN	40.07 (40.21)	3.45 (3.07)	9.68 (10.66)	8.87 (8.93)	7.90 (7.91)	1.0 MeCN
DAZOP[CuCr(ox)$_3$]·MeCN	39.92 (39.32)	3.05 (2.91)	10.58 (9.83)	9.60 (9.91)	7.85 (8.11)	0.80 MeCN

compounds. They are consistent with a general formulation A[M^{II}Cr(ox)$_3$]·*n* solv. Some of the compounds retain solvent molecules (methanol or acetonitrile). Thermogravimetric analyses have shown that the imprisoned solvent is released over the temperature range 40−200 °C. The solvent contents given in Table 1 are based on thermogravimetric determinations.

The compounds crystallized as very fine powders with particle size about 1 μm. Numerous efforts at growing single crystals of A[M^{II}Cr(ox)$_3$] suitable for X-ray structure determination were successful only with M^{II} = Mn and A = MIPS, DAPS. Single crystals of DAPS[MnCr(ox)$_3$].CH$_3$CN were obtained in a "one pot" synthesis by dissolving at room temperature equimolar amounts (0.2 mmol) of (DAPS)NO$_3$, [K$_3$Cr(ox)$_3$]·3H$_2$O, and Mn(NO$_3$)$_2$·4H$_2$O in 3 mL of a (1:1:1) mixture of water, methanol, and acetonitrile (2 days standing). Single crystals of MIPS[MnCr(ox)$_3$] were obtained similarly by dissolving equimolar amounts (0.2 mmol) of (MIPS)Br, [K$_3$Cr(ox)$_3$]·3H$_2$O and Mn(NO$_3$)$_2$·4H$_2$O in a (1:2) mixture of water (9 mL) and methanol (18 mL).

Infrared spectra were obtained (FTIR Spectrum 1000 Perkin-Elmer spectrometer) using powdered samples pressed in KBr pellets. UV−visible spectra were obtained with a Varian Cary 5E spectrometer. X-ray powder diffraction patterns were obtained with a Siemens diffractometer equipped with a rear monochromator, using Cu Kα radiation. Indexation of the diffraction peaks was carried out using DicVol91 software.[26]

Non linear optical measurements were carried out at room temperature using the Kurtz−Perry powder technique.[27] The 1.064 μm wavelength laser radiation, obtained from a ps Nd:YAG pulsed (10 Hz) laser, was passed through a 1 m long cell containing hydrogen gas under a pressure of 50 bar, to generate the 1.907 μm radiation used for measurements. Samples consist of microcrystalline powder squeezed between two glass plates. After passing through appropriate filters, the transmitted signal was detected by a photomultiplier and visualized on an ultrafast Tektronix 7834 oscilloscope. The second harmonic signals were calibrated with respect to a sieved urea sample.

Magnetic measurements were carried out on powder samples with a Quantum Design SQUID magnetometer operating in *dc* mode down to 2 K. The ($\chi_M T$) versus T curves, χ_M being the molar magnetic susceptibility per A[M^{II}Cr^{III}(ox)$_3$] group, were recorded with a magnetic field of 1 kOe. An average diamagnetic correction of 440 × 10^{-6} emu mol^{-1} was estimated for all compounds.

Crystallographic Data Collection and Refinement of the Structures. A block-shaped dark-red crystal of DAPS[MnCr(ox)$_3$]·CH$_3$CN with dimensions 0.20 × 0.25 × 0.40 mm and an extremely thin needle-shaped bright-red crystal of MIPS[MnCr(ox)$_3$] with dimensions 0.06 × 0.25 × 0.40 mm were chosen for X-ray diffraction experiments. The first one was mounted in a sealed glass capillary with 0.3 mm diameter, to avoid solvent losses.

A preliminary data collection on an ENRAF NONIUS CCD-based diffractometer (50 kV and 30 mA) at room temperature with Mo Kα radiation indicated the monoclinic symmetry of both crystals. The reflections covered a full sphere of reciprocal space, the crystal-to-detector distance was 40 mm, each frame covered 1.9° (in ω) for 47 s/deg exposure time for DAPS[MnCr(ox)$_3$]·CH$_3$CN and 0.7° with an integration time of 190 s/deg for MIPS[MnCr(ox)$_3$]. The complete data-collection strategy and crystallographic details are summarized in Table 2. Cell parameters were retrieved using Kappa CCD software.[28] Data reduction was performed using the same software. The procedure of integration of frames is described by Kabsch.[29] Both structures were solved by direct methods using the SHELXS86 program[30] and refined with SHELXL93.[31] The drawings were prepared with ORTEPII.[32]

Table 2. Crystal Data and Structure Refinement for DAPS[MnCr(ox)$_3$]·CH$_3$CN and MIPS [MnCr(ox)$_3$]

compound	DAPS[MnCr(ox)$_3$]·CH$_3$CN	MIPS[MnCr(ox)$_3$]
formula	$C_{26}H_{26}N_3O_{12}MnCr$	$C_{25}H_{24}NO_{13}MnCr$
fw	679.44	653.39
temp (K)	293	293
crystal system	monoclinic	monoclinic
space group	$P2_1/c$	$P2_1/c$
a (Å)	9.5274(2)	9.535(1)
b (Å)	15.7802(4)	15.890(2)
c (Å)	20.4054(4)	18.229(9)
α (deg)	90	90
β (deg)	76.510(1)	83.810(9)
γ (deg)	90	90
V (Å^3)	2983.2(1)	2745.8(5)
Z	4	4
d_x (Mg/m^3)	1.502	1.581
μ (mm^{-1})	0.853	0.924
F(000)	1372	1336
crystal size (mm)	0.20 × 0.25 × 0.40	0.06 × 0.25 × 0.40
Θ range (deg)	2.20 to 25.08	1.70 to 21.90
index ranges	$-11 \le h \le 11$	$-9 \le h \le 9$
	$-18 \le k \le 18$	$-15 \le k \le 15$
	$-24 \le l \le 24$	$-16 \le l \le 16$
$N_{collect}$	10348	4261
N_{indt}	5287 [R(int) = 0.0227]	2310 [R(int) = 0.0222]
N_{obs}	4209 [$I > 2\sigma(I)$]	1937 [$I > 2\sigma(I)$]
R1 [$I > 2\sigma(I)$]	0.0498	0.0507
wR2	0.1091	0.1037

Both complexes crystallized in the monoclinic space group $P2_1/c$. Compound DAPS[MnCr(ox)$_3$]·CH$_3$CN comprises the 2-dimensional [MnCr(ox)$_3$]$^-$ anionic network, DAPS cations and acetonitrile molecules. The anionic oxalate network could be assigned without any difficulties and refined anisotropically. However the DAPS species are

(26) Louer, D.; Louer, M. *J. Appl. Crystallogr.* **1972**, *5*, 271; Boultif, A.; Louer, D. *J. Appl. Crystallogr.* **1991**, *24*, 987.
(27) Kurtz, S. K.; Perry, T. T. *J. Appl. Phys.* **1968**, *39*, 3798.
(28) Enraf Nonius Kappa CCD. *User's Manual*, revision 1.10.
(29) Kabsch, W. *J. Appl. Crystallogr.* **1993**, *26*, 795−800.
(30) Sheldrick, G. M. *SHELXS86*. Program for the solution of crystal structures. University of Göttingen: Germany, 1986.
(31) Sheldrick, G. M. *SHELXL93*. Program for the refinement of crystal structures. University of Göttingen: Germany, 1993.
(32) Johnson, C. K. *ORTEPII*. Report ORNL-5138. Oak Ridge National Laboratory: Tennessee, 1976.

Scheme 2. Superposition of Two Parts of Disordered DAPS Cation: Solid Lines Represent the Major Part (80%) and Dashed Lines the Minor Part (20%)

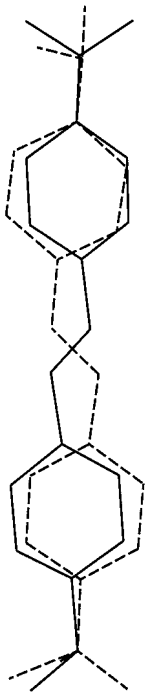

orientationally disordered. In the nonsolved structure the observed length of the "central" C═C bond is found much shorter than the true length, whereas the two adjacent C−C(Ph) bonds are much longer. This observation is a definite proof of the presence of disorder. Two disordered parts of one DAPS species are approximately related to one another by a 180° rotation around the long axis (Scheme 2). This orientational disorder could not be resolved if the usual refinement and difference Fourier synthesis were used. This is probably due to a low population of the misoriented molecule. The extent of misorientation was determined to be 20%. The two disordered parts of molecule DAPS were refined with a "similarity restraint" (SAME). The structure (comprising the anionic layers, the major part of the disordered cations and the non-hydrogen atoms of the solvent molecules) was refined anisotropically by full-matrix least-squares approximation based on F^2. The minor part of the disordered cation was refined isotropically. Hydrogen atom positions were calculated by assuming geometrical positions and were included in the structural model. Final weighting scheme was $w = 1/[\sigma^2(F_o^2) + (0.0369)^2 + 3.4051P]$, where $P = (F_o^2 + 2F_c^2)/3$. The final refinement of this model was continued until convergence when $R1 = 0.0498$ for $F^2 > 2\sigma(F^2)$ and $R_w = 0.1008$. The final difference map showed the largest residual peaks of 0.275 and −0.324 eÅ^{-3}.

Resolution of the structure of MIPS[$MnCr(ox)_3$] from the complete data set was not trivial. Reflections in reciprocal space showed systematic absences characteristic of the $P2_1/c$ space group: $0k0$, $k = 2n + 1$ and $h0l$, $l = 2n + 1$ absent. However solutions to the phase problem could not be obtained in this group. A structure was found in *Pc* space group, and anisotropic refinement led to an *R*-value 0.044. A strong structural relationship was observed between the atomic coordinates in both molecular entities, the metallic cluster and two MIPS molecules. The space group assignment was evidently not correct. We obtained an asymmetric part of the anion and the cation in centrosymmetric space group by symmetry transformation and the structure was refined anisotropically (non-hydrogen atoms) by full-matrix least-squares approximation based on F^2 in $P2_1/c$ space group.

In contrast to the DAPS[$MnCr(ox)_3$]·CH_3CN structure, there was no indication of disorder in MIPS[$MnCr(ox)_3$]. Hydrogen atom positions were found in difference Fourier maps and were isotropically refined. Final weighting scheme was $w = 1/[\sigma^2(F_o^2) + (0.0010)^2 + 9.0101P]$, where $P = (F_o^2 + 2F_c^2)/3$. The final refinement of this model was continued until convergence when $R1 = 0.0507$ for $F^2 > 2\sigma(F^2)$ and $R_w = 0.1037$. The final difference map showed the largest residual peaks of 0.273 and −0.259 eÅ^{-3}. The observed high-temperature factors of the terminal ethyl group indicate a low accuracy in the determination of the position of the C10 and C11 atoms. This might arise from partial disorder of ethyl groups, but the refinement of a model based on disorder was unsuccessful. Consequently, we attributed the high-temperature factors to strong thermal vibrations of the atoms.

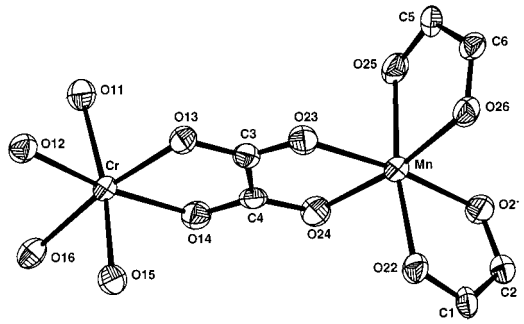

Figure 1. ORTEP drawing (30% probability) of the Mn and Cr coordination sphere in the two-dimensional network.

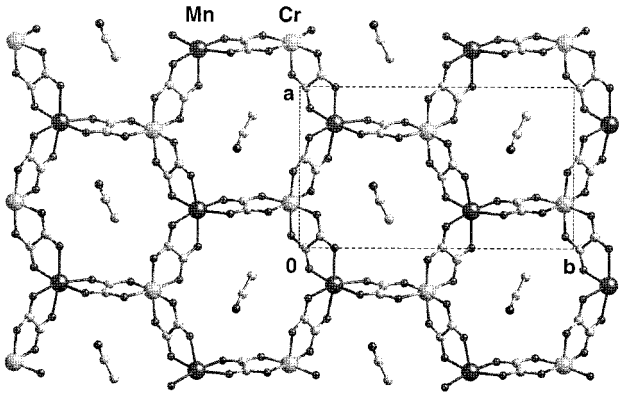

Figure 2. Representation of the $[MnCr(ox)_3]_n^{n-}$ layer with the CH_3CN molecule inclusion in hexagonal cavities in DAPS[$MnCr(ox)_3$]·CH_3CN.

Results and Discussion

Structure of DAPS[$MnCr(ox)_3$]·CH_3CN and MIPS[$MnCr(ox)_3$]. Compounds DAPS[$MnCr(ox)_3$]·CH_3CN and MIPS[$MnCr(ox)_3$] are isostructural if one neglects the chromophore substituents and the solvent molecule. Both structures belong to the centrosymmetric $P2_1/c$ space group with $Z = 4$, and have very similar cell constants (Table 2). The **c** parameter is larger by 2.2 Å in the DAPS[$MnCr(ox)_3$]·CH_3CN structure than in the MIPS analogue, and the angle β decreases by 7.3°. These two structures are examples of a specific phenomenon that may be called "homologous isomorphism".[33] The crystal structure confirms the 1:1:1 molar ratio of anion to cation and solvent in DAPS[$MnCr(ox)_3$]·CH_3CN and the 1:1 ratio of anion to cation in MIPS[$MnCr(ox)_3$] which does not contain any solvent molecules. The crystal structures of both compounds consists of bimetallic anionic layers with stoichiometry $[MnCr(ox)_3]_n^{n-}$ which alternate with layers of DAPS (or MIPS) counterions along the **c** direction.

The Bimetallic $[MnCr(ox)_3]_n^{n-}$ Layers. A view of the trimeric anionic $[MnCr(ox)_3]^-$ unit, including atom labeling, is shown in Figure 1. The ORTEPII diagrams of these units in both compounds are indistinguishable to the eye, hence only one is shown. These units form a slightly distorted hexagonal pattern along the layer plane, represented in Figure 2 in the

(33) Kitaigorodsky, A. I. *Molecular Crystals and Molecules*; Academic Press: New York and London, 1973.

Table 3. Selected Bond Lengths [Å] and Angles [deg] for DAPS[$MnCr(ox)_3$]·CH_3CN and MIPS[$MnCr(ox)_3$] Complexes

DAPS[$MnCr(ox)_3$]·CH_3CN				MIPS [$MnCr(ox)_3$]			
Cr−O(11)	1.982(2)	Mn−O(21)	2.186(2)	Cr−O(11)	2.059(5)	Mn−O(21)	2.088(5)
Cr−O(12)	1.975(2)	Mn−O(22)	2.183(2)	Cr−O(12)	2.068(5)	Mn−O(22)	2.086(5)
Cr−O(13)	1.970(2)	Mn−O(23)	2.185(2)	Cr−O(13)	2.065(5)	Mn−O(23)	2.087(5)
Cr−O(14)	1.969(2)	Mn−O(24)	2.173(2)	Cr−O(14)	2.061(5)	Mn−O(24)	2.121(5)
Cr−O(15)	1.974(2)	Mn−O(25)	2.200(2)	Cr−O(15)	2.053(5)	Mn−O(25)	2.065(5)
Cr−O(16)	1.973(2)	Mn−O(26)	2.165(2)	Cr−O(16)	2.070(5)	Mn−O(26)	2.107(5)
O(12)−Cr−O(11)	83.18(9)	O(22)−Mn−O(21)	76.53(8)	O(11)−Cr−O(12)	80.1(2)	O(21)−Mn−O(22)	79.5(2)
O(13)−Cr−O(11)	93.60(10)	O(23)−Mn−O(21)	167.10(9)	O(11)−Cr−O(13)	93.2(2)	O(21)−Mn−O(23)	170.8(2)
O(14)−Cr−O(11)	92.59(9)	O(24)−Mn−O(21)	101.76(9)	O(11)−Cr−O(14)	96.9(2)	O(21)−Mn−O(24)	91.9(2)
O(15)−Cr−O(11)	171.74(10)	O(25)−Mn−O(21)	94.61(9)	O(11)−Cr−O(15)	171.0(2)	O(21)−Mn−O(25)	94.4(2)
O(16)−Cr−O(11)	91.18(10)	O(26)−Mn−O(21)	91.36(10)	O(11)−Cr−O(16)	96.7(2)	O(21)−Mn−O(26)	94.9(2)
O(13)−Cr−O(12)	94.01(9)	O(23)−Mn−O(22)	90.68(9)	O(12)−Cr−O(13)	91.7(2)	O(22)−Mn−O(23)	98.5(2)
O(14)−Cr−O(12)	174.82(10)	O(24)−Mn−O(22)	95.34(10)	O(12)−Cr−O(14)	170.9(2)	O(22)−Mn−O(24)	93.5(2)
O(15)−Cr−O(12)	91.11(9)	O(25)−Mn−O(22)	171.14(9)	O(12)−Cr−O(15)	91.4(2)	O(22)−Mn−O(25)	170.9(2)
O(16)−Cr−O(12)	91.51(10)	O(26)−Mn−O(22)	102.95(10)	O(12)−Cr−O(16)	90.6(2)	O(22)−Mn−O(26)	94.2(2)
O(14)−Cr−O(13)	83.24(9)	O(24)−Mn−O(23)	77.53(8)	O(13)−Cr−O(16)	170.1(2)	O(23)−Mn−O(26)	94.1(2)
O(13)−Cr−O(15)	92.76(9)	O(23)−Mn−O(25)	98.18(9)	O(14)−Cr−O(13)	79.9(2)	O(24)−Mn−O(23)	79.2(2)
O(13)−Cr−O(16)	173.10(10)	O(23)−Mn−O(26)	93.11(9)	O(14)−Cr−O(16)	98.2(2)	O(25)−Mn−O(24)	93.6(2)
O(14)−Cr−O(15)	93.40(10)	O(24)−Mn−O(25)	86.29(9)	O(15)−Cr−O(13)	90.0(2)	O(25)−Mn−O(23)	88.5(2)
O(16)−Cr−O(15)	82.97(9)	O(26)−Mn−O(25)	77.03(9)	O(15)−Cr−O(14)	92.0(2)	O(26)−Mn−O(24)	170.5(2)
O(14)−Cr−O(16)	91.57(10)	O(24)−Mn−O(26)	159.59(9)	O(15)−Cr−O(16)	80.3(2)	O(25)−Mn−O(26)	79.4(2)

Table 4. Intermolecular Contacts (≤3.6 in Å) for DAPS[$MnCr(ox)_3$]·CH_3CN and MIPS[$MnCr(ox)_3$]

DAPS[$MnCr(ox)_3$]·CH_3CN		MIPS[$MnCr(ox)_3$]			
atoms[a]	distances	atoms[b]	distances		
solvent−anion		cation−cation			
N1S−O14(i)	3.553	C12−C21(i)	3.505	C22−C23(ii)	3.479
N1S−O15(i)	3.356	C13−O(i)	3.334	O−O(iii)	3.117
N1S−C5(i)	3.120	C21−C12(ii)	3.505	O−C20(iii)	3.417
N1S−O25(i)	3.230	C22−C24(ii)	3.456		
atoms[a]	distances	atoms[c]	distances		
cation−anion					
C7−O26(ii)	3.581	C12−O12(i)	3.558		
C8−O15(iii)	3.465	C12−O13(i)	3.333		
C9−O15(iii)	3.392	C13−O22(ii)	3.256		
C13−O11(iv)	3.519	C14−O26(iii)	3.602		
C16−O23(iv)	3.600	C16−O11(iv)	3.458		
C23−O16(iv)	3.349	C22−O15(v)	3.309		
C26−O25(v)	3.476	C23−O13(iv)	3.518		
C26−O21(vi)	3.422	C23−O23(iv)	3.509		
C25−O24(vi)	3.555	C31−O22(iv)	3.572		
C29−O12(vi)	3.483				

[a] Symmetry operations for second atom: (i) $-X+1, Y+0.5, -Z+0.5$; (ii) $X-1, -Y+1.5, Z+0.5$; (iii) $X-1, Y+1, Z$; (iv) $-X, Y+0.5, -Z+0.5$; (v) $-X, -Y+1, -Z+1$; (vi) $X, -Y+1.5, Z+0.5$. [b] Symmetry operations for second atom: (i) $X+1, Y, Z$; (ii) $-X+1, -Y+1, -Z$; (iii) $-X, -Y+1, -Z$. [c] Symmetry operations for second atom: (i) $X+1, -Y+0.5, Z-0.5$; (ii) $-X+1, -Y+1, -Z$; (iii) $X-1, Y, Z$; (iv) $-X+2, -Y, -Z$; (v) $-X, -Y+1, -Z$.

particular case of DAPS[$MnCr(ox)_3$]·CH_3CN, where acetonitrile molecules are occluded within the intralayer cavities, see below. Selected bond distances and angles for DAPS[$MnCr(ox)_3$]·CH_3CN and MIPS[$MnCr(ox)_3$] are listed in Table 3. Although the **a** and **b** parameters of both compounds are almost identical, there are significant differences in the metal oxygen distances. In DAPS[$MnCr(ox)_3$]·CH_3CN the metal to oxygen distances at the M^{II} sites are significantly longer than those at the Cr^{III} sites (mean value of Mn−O distances around 2.17 Å, mean value of Cr−O distances around 1.97 Å). This difference is much smaller in MIPS[$MnCr(ox)_3$]: the mean value of Mn−O distances decreases to 2.09 Å, while the mean value of the Cr−O distances reaches 2.06 Å.

Another structural aspect of DAPS[$MnCr(ox)_3$]·CH_3CN deserves some comment. One acetonitrile molecule is enclathrated in every cavity of the anionic layer as an equatorial inclusion, forming a two-dimensional host−guest system (Figure 2). As the cavity dimensions match the van der Waals size of the acetonitrile molecules, the presence of the latter in the DAPS[$MnCr(ox)_3$]·CH_3CN compound does not influence the **c** parameter. The stabilization of the CH_3CN molecule in the cavity is associated with short contacts between the nitrogen atoms of acetonitrile and the oxygen atoms of the oxalate ligands (Table 4). Orientation of the CH_3CN molecules coincides with the pseudo-axis between the opposite Cr···Mn atoms, the nitrogen atom being positioned toward the Mn atom. This orientation apparently amplifies the difference between the Cr and Mn sites.

Molecular Arrangement along One Chromophore Layer. The molecular structure and atom labeling of DAPS and MIPS is shown in Figure 3. As already mentioned, the DAPS molecules in the oxalate compound are orientationally disordered, and only the major part will be taken into consideration. The DAPS and MIPS molecules once intercalated have a twisted conformation, the dihedral angle between the benzene and pyridinium rings being 13.3° and 30.8° for DAPS and MIPS, respectively. The ethylene-like central part of the included DAPS species is nearly coplanar with the benzene ring, while the

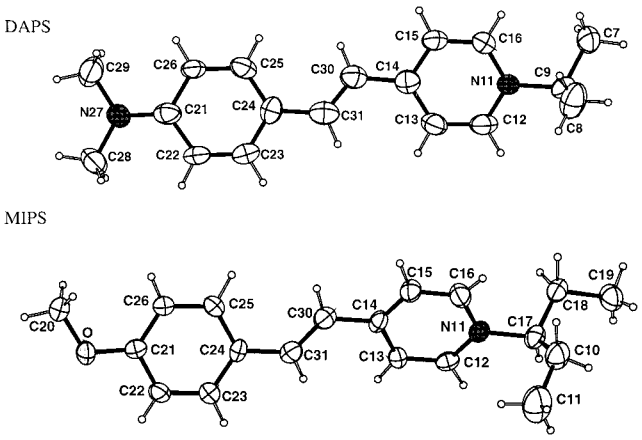

Figure 3. ORTEP drawing of the cationic chromophores DAPS and MIPS. Only the major component of DAPS with the population of 80% is shown. The molecules are shown in the same orientation. The ellipsoids correspond to 30% probability contours of atomic displacement. H atoms have been given arbitrary radii.

pyridine ring is twisted away from this plane by a torsion angle C31−C30−C14−C13 of 9.8°. In the case of the MIPS cation, rotation takes place about both the C30−C14 and C24−C31 bonds with torsion angles of 12.5 and 21.4°, respectively.

Beside these conformational differences between the DAPS and MIPS chromophores, major differences are observed between their packing mode. The DAPS molecules are oriented essentially "edge-on" between the oxalate layers, with their "principal axes" all parallel to the diagonal direction of the rectangular (**a**, **b**) cell. They form rows running along the **a** axis and the midpoint of the C═C bond of one molecule faces the center of the benzene ring of the adjacent molecule. However, the dipolar moments of two adjacent "face-to-face" DAPS cations (along the **a** axis) have antiparallel orientations (Figure 4a). There are no intermolecular distances shorter than usual van der Waals contacts.

Because of their more twisted conformation, the MIPS cations cannot be described as being oriented "edge-on". The plane of the aromatic cycles considerably deviate from perpendicularity with respect to the oxalate layers, hence the lower basal spacing (9.06 vs 9.92 Å for DAPS). Although the long axes of the MIPS species are mutually parallel (as for DAPS), the arrangement of their dipolar moments within the interlayer region is different. The MIPS chromophores still form rows running along the **a** axis, but the dipolar moments of the molecules located along the row are lined up. However, the dipolar moments along two adjacent rows are antiparallel (Figure 4b). In contrast to DAPS, short interatomic distances between adjacent MIPS molecules are observed, which involve attractive "face-to-face" $\pi-\pi$ interactions between parallel aromatic rings and "edge-to-face" interactions between perpendicularly oriented aromatic rings (Table 4).

Organization and Interactions along the Stacking Direction. Side views of the structure of DAPS$[MnCr(ox)_3].CH_3CN$ and of MIPS$[MnCr(ox)_3]$ are shown in Figure 5a and 5b, respectively. Along the stacking direction in both cases, two successive $[MnCr(ox)_3]_n^{n-}$ layers are separated by a distance corresponding to $^1/_2$ of the true **c** parameter. Several features are associated with the superstructure:

(i) The $[MnCr(ox)_3]_n^{n-}$ layers are stacked according to an ABAB mode. In MIPS$[MnCr(ox)_3]$, the Mn^{II} ions of one layer lie directly over those of the next one but the Cr^{III} ions of one layer lie over the center of the cavities of the next layer. In DAPS$[MnCr(ox)_3]\cdot CH_3CN$, the metal sites of one layer are almost in registry with those of the next layer, but these metal sites are occupied by ions of different nature (Cr···Mn···Cr··· Mn sequence)

(ii) The chirality around the metallic ions is inverted on going from one layer to the next one. If the $[Mn(ox)_3]^{4-}$ units in one layer are Δ (and hence the $[Cr(ox)_3]^{3-}$ are Λ), then the $[Mn(ox)_3]^{4-}$ units in the adjacent layer will be Λ (and hence the $[Cr(ox)_3]^{3-}$ Δ)

(iii) The long axes of the MIPS chromophores belonging to successive layers are nearly perpendicular to each other (84° between the axes). This angle drops to 72° in the case of the DAPS chromophores.

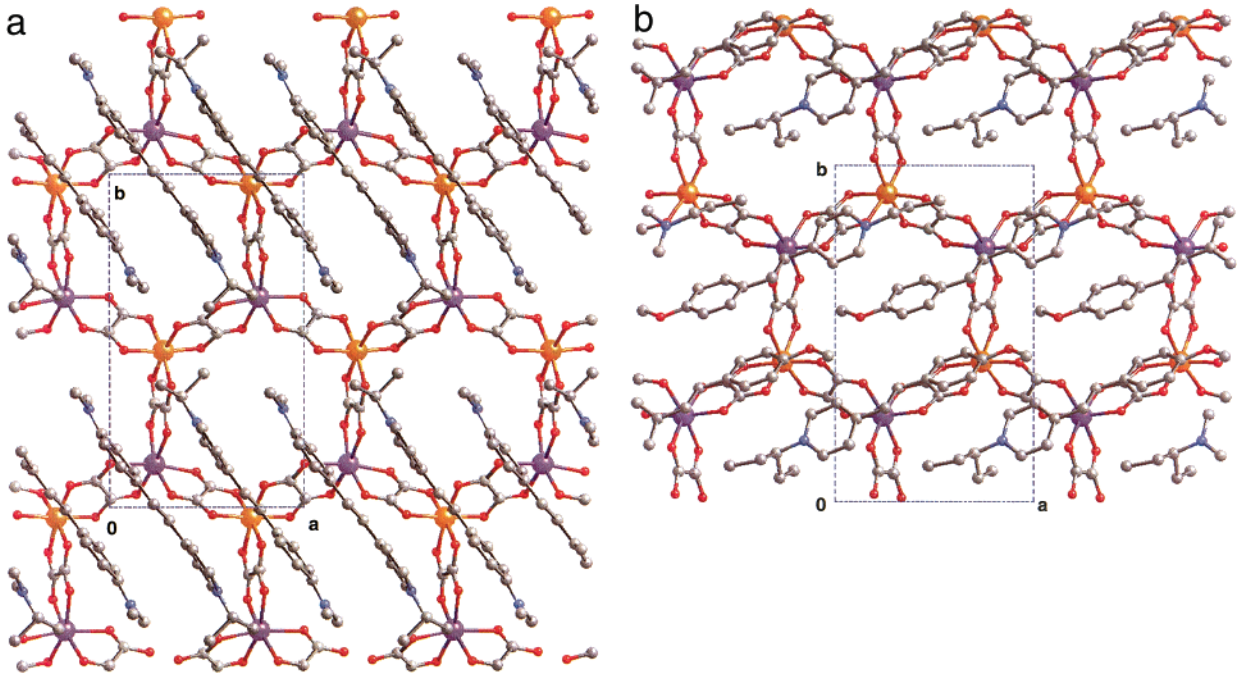

Figure 4. Top view of the structure of (a) DAPS$[MnCr(ox)_3]\cdot CH_3CN$ and (b) MIPS$[MnCr(ox)_3]$ along the (**a**, **b**) plane. Only one layer of oxalate and one layer of chromophores are shown. The occluded acetonitrile molecules in (a) have been omitted.

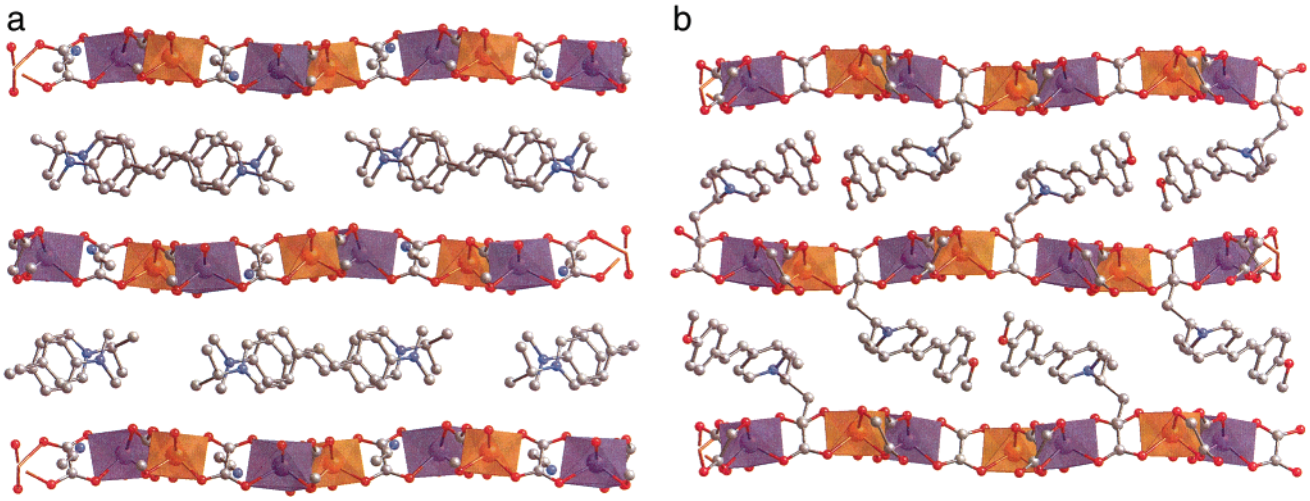

Figure 5. Side view of the structure of (a) DAPS[MnCr(ox)$_3$]·CH$_3$CN and of (b) MIPS[MnCr(ox)$_3$] along the stacking direction.

Other features are of interest. The *gauche* oriented ethyl groups of the MIPS molecules (see Figure 5b) slightly penetrate the [MnCr(ox)$_3$]$^-$ cavities of the two surrounding upper and lower inorganic layers, a feature which is certainly related to the absence of encapsulated solvent in these cavities (steric hindrance). Finally, the packing between the chromophores and the oxalate layers in both structures is characterized by the short interatomic contacts between the carbon atoms of the cations (DAPS or MIPS) and the oxygen atoms of the oxalate ligands (Table 4).

Structural Characterization of the Other A[M^{II}Cr(ox)$_3$] Compounds. In addition to the analytical data mentioned in the Experimental Section, the 35 compounds A[M^{II}Cr(ox)$_3$]·*n* solv synthesized in this work have been characterized by infrared spectroscopy and X-ray powder diffraction.

The infrared spectra of the compounds show numerous sharp bands attributable in each case to the particular chromophore included and to the oxalate groups. The characteristic antisymmetric ν(CO) stretching mode systematically appears as a single intense band around 1630 cm^{-1}, indicating that all of the oxalate groups act as bridging ligands. This feature is consistent with the above-described structure of the oxalate layers.

X-ray powder diffraction patterns have been obtained for all the compounds. Examination of the width of the reflections reveals that the various compounds present different degrees of crystallinity. A few representative X-ray profiles are given in Figure 6 for the highly crystalline DAZOP[MnCr(ox)$_3$], the somewhat less crystalline DAMS[NiCr(ox)$_3$] and the quite disordered CINDAMS[MnCr(ox)$_3$]. A qualitative indication of the crystallinity of each compound is appended in Table 5. Indexation of the diffraction patterns was achieved only in the case of well-crystallized compounds, which typically exhibit about 15−20 lines over the range 9°−35° (2θ). In contrast to most ammonium of phosphonium compounds previously studied in the same family, no indexation could be found in the hexagonal system. The diffraction patterns of the best crystalline compounds (see Table 5) were indexed using a monoclinic unit cell with parameters gathered in Table 6. Although the validity of any indexation of a powder pattern in the monoclinic system is questionable, the values of the **a** and **b** parameters shown in Table 6 appear to be reliable for the following reasons: (i) The values of **a** and **b** are very close to those derived from the single crystal study of MIPS (or DAPS)[MnCr(ox)$_3$]. This strongly suggests that the compounds synthesized in this work are structurally very close to the layered oxalates already known.

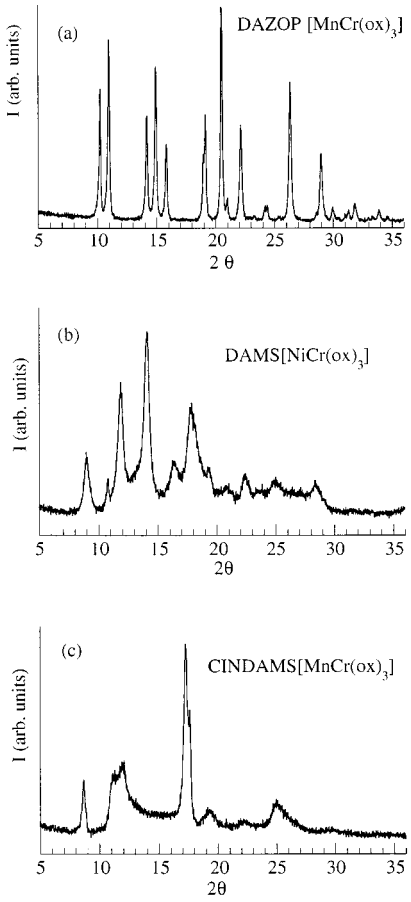

Figure 6. X-ray powder diffraction profiles of three compounds having different crystallinity: (a) DAZOP[MnCr(ox)$_3$]·0.5CH$_3$CN, (b) DAMS [NiCr(ox)$_3$], (c) CINDAMS [MnCr(ox)$_3$].

(ii) On going from Mn^{II} to Cu^{II} in a series of A[M^{II}Cr(ox)$_3$] compounds possessing the same chromophore A, a monotonic decrease of **a** and **b** is systematically observed, which parallels the variation of the ionic radii of the metallic M^{II} ions. (iii) The same *hkl* reticular planes appear in the various indexations.

In contrast, the **c** parameters found are 2 times smaller than the values derived from the single crystal study of MIPS (or DAPS)[MnCr(ox)$_3$], that is, no superstructure is apparent along the stacking direction. However, this result cannot be taken for granted, because it is possible that weak superstructure reflections be missed on the powder spectra.

Table 5. Characteristic Features of the $A[MCr(ox)_3]$ Compounds Synthesized in This Work: Second Harmonic Generation (SHG) Relative to Urea, Qualitative Indication of the Crystallinity (Cryst), Basal Spacing (BS)

		DAZOP	DAMS	DAES	DAPS	MIPS	MHS	CINDAMS
$[MnCr(ox)_3]$	SHG	100	100	0	0	0	30	40
	cryst.	high	high	high	high	high	high	low
	BS (Å)	8.63	8.77	9.44	9.92	9.06	9.69	10.2
$[FeCr(ox)_3]$	SHG	19	17	5	19	4	21	10
	cryst.	high	high	high	high	medium	high	low
	BS (Å)	8.69	8.84	9.67	10.04	9.5	9.77	10.4
$[CoCr(ox)_3]$	SHG	100	10	0	7	6	0	21
	cryst.	high	high	medium	medium	low	low	low
	BS (Å)	8.72	8.91	10.2	10.4	9.5	10.3	10.5
$[NiCr(ox)_3]$	SHG	25	25	0	0	0	0	1
	cryst.	low	medium	low	low	low	low	low
	BS (Å)	10.7	9.9	10.3	10.4	10.3	10.6	10.5
$[CuCr(ox)_3]$	SHG	32	10	0	1	0	0	8
	cryst.	high	high	high	high	high	low	low
	BS (Å)	8.80	9.01	10.17	10.12	9.40	10.4	10.5

Table 6. Parameters of the Monoclinic Unit Cell of Selected $A[MCr(ox)_3]$ Compounds

compound	*a* (Å)	*b* (Å)	*c* (Å)	β (deg)
$DAZOP[MnCr(ox)_3]$	9.332(4)	16.250(8)	8.717(4)	97.21(4)
$DAZOP[FeCr(ox)_3]$	9.149(9)	16.205(24)	8.776(5)	96.90(8)
$DAZOP[CoCr(ox)_3]$	8.963(3)	16.204(8)	8.790(3)	96.52(3)
$DAZOP[CuCr(ox)_3]$	8.903(4)	16.176(14)	8.856(7)	96.55(5)
$DAMS[MnCr(ox)_3]$	9.048(4)	16.685(9)	8.845(6)	96.74(8)
$DAMS[FeCr(ox)_3]$	8.823(8)	16.626(10)	8.867(5)	95.83(7)
$DAMS[CoCr(ox)_3]$	8.718(3)	16.548(10)	8.954(4)	95.98(4)
$DAMS[CuCr(ox)_3]$	8.686(6)	16.537(14)	9.034(8)	96.39(8)
$DAPS[MnCr(ox)_3]$*	9.5274(1)	15.7802(4)	20.4054(4)	103.490(1)
$MIPS[MnCr(ox)_3]$*	9.535(1)	15.890(2)	18.229(9)	83.810(9)

[a] Values extracted from single-crystal X-ray determination (see text).

The X-ray patterns of the less crystalline compounds synthesized in this work always exhibit, among other broad reflections, two rather sharp reflections which can be indexed as 001 and 002 and which are therefore characteristic of the basal spacing. The values are gathered in Table 5. Examination of Table 5 reveals that, in any column corresponding to a given chromophore, the more disordered character of a compound is associated to a significantly larger basal spacing.

NLO Properties. The efficiency of the 35 $A[M^{II}Cr(ox)_3]$ compounds at second harmonic generation (SHG) has been measured, and the data are reported in Table 5. About two-thirds of these compounds are NLO active, and a few (particularly those containing DAMS and DAZOP) are even very efficient. The large SHG response may be due in part to a resonant excitation, but the large difference between the second harmonic wavelength (0.95 μm) and the absorption wavelengths of DAZOP and DAMS (0.4−0.55 μm) should keep resonant effects rather small. One-third of the compounds are totally inactive. Examination of Table 5 does not suggest any obvious correlation between the NLO efficiency and the crystallinity of the materials. Several compounds are rather efficient despite a low crystallinity, for example $CINDAMS[MnCr(ox)_3]$, while others are inactive despite high crystallinity, for example MIPS (and DAPS)$[MnCr(ox)_3]$. Although there is not an overall correlation between the interlayer distance of the compounds and their SHG efficiency, it is remarkable that the three most active compounds also have particularly short interlayer distances. The relationship between the interlayer distance and the NLO activity will be further discussed later in the text.

It should be emphasized that small modifications of the synthetic methods may exert a crucial role on the NLO properties. Thus, when $DAZOP[FeCr(ox)_3]$ was prepared using a (1:1) methanol−acetonitrile mixture as the solvent, the powder obtained was poorly crystallized and showed SHG efficiency of 0.3 only. However, when a small amount of water was added to the solvent during the synthesis (2:12:12 water, methanol, acetonitrile), the compound obtained was far more crystalline and showed SHG efficiency 19 times stronger than urea. Therefore, the values of efficiency given in Table 5 should be considered as minimal values, and some of them may be possibly improved by optimizing the synthesis.

Magnetic Properties. All $A[M^{II}Cr(ox)_3]$ compounds prepared in this work present similar magnetic properties, that is, they all show ferromagnetic interactions which lead to ferromagnetic ordering below a Curie temperature which depends on the nature of the M^{II} ion. The Curie temperatures range from about 6 K (M = Mn) to about 14 K (M = Co, Ni). The data are consistent with previous studies on layered bimetallic oxalates possessing ammonium or phosphonium cations. Because of the large number of compounds studied, we restrict the presentation to some representative SHG efficient compounds (with M = Mn, Fe, Co, Ni, Cu) and to the inactive $DAPS[MnCr(ox)_3]$ compound taken as a reference.

$DAZOP[MnCr(ox)_3]$. The $\chi_M T$ product for this compound at room temperature is equal to 6.55 emu·K·mol^{-1}, slightly larger than the value (6.25 emu·K·mol^{-1} if $g = 2$) expected for non-interacting Mn^{II} and Cr^{III} magnetic centers with the local spins $S_{Mn} = {}^5/_2$ and $S_{Cr} = {}^3/_2$. As T is lowered, $\chi_M T$ increases more and more rapidly. The field dependence of the magnetization, $M = f(H)$, at 2 K shows a rapid increase of M and a saturation regime at higher fields with a saturation magnetization of about 7.2 $N\beta$, very close to the value expected for a parallel alignment of the Mn^{II} and Cr^{III} magnetic moments. The temperature dependence of the field-cooled, remnant, and zero field-cooled magnetizations are shown in Figure 7a. These curves are typical of a ferromagnetic material with a weak remnant and a Curie temperature of about 6 K.

$DAPS[MnCr(ox)_3]\cdot CH_3CN$. It is interesting to compare the magnetic properties of this SHG inactive compound with those of the active DAMS analogue described above. The general behavior is the same, but some differences are significant. At room temperature $\chi_M T$ for $DAPS[MnCr(ox)_3]\cdot CH_3CN$ is equal to 6.35 emu·K·mol^{-1}, that is exactly the value expected for non-interacting Mn^{II} and Cr^{III} ions. The compound also orders ferromagnetically below 6 K. However The $M = f(H)$ curve of the DAPS compound shows an extremely rapid increase of M, steeper than with DAMS, even though the saturation values are the same. Another difference can be seen on the M(T) curve under low or zero field: the remnant magnetization of DAPS-

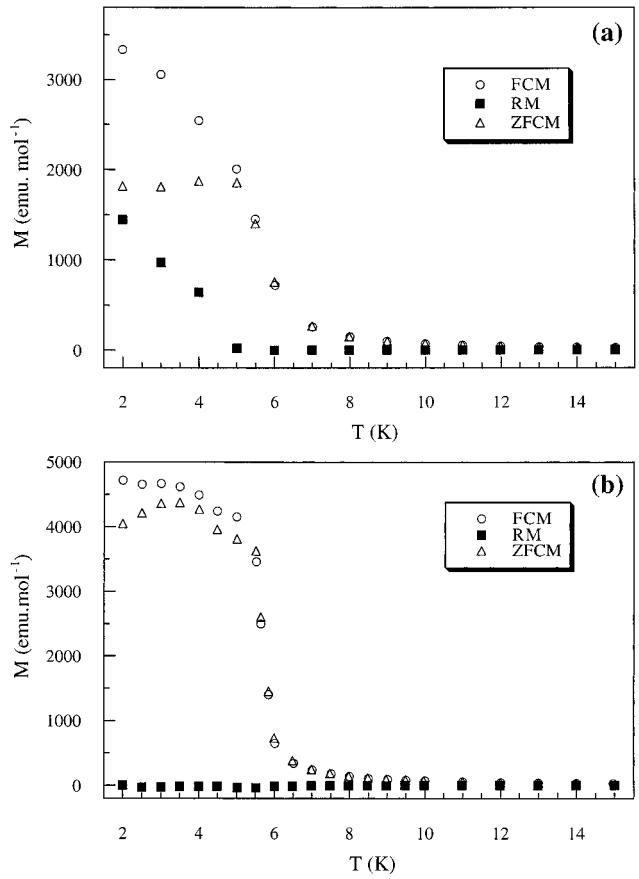

Figure 7. Temperature dependence of the magnetization M of (a) DAZOP[MnCr(ox)$_3$]·0.5CH$_3$CN, (b) DAPS[MnCr(ox)$_3$]; (○) field-cooled magnetization (FCM) (30 G); (■) remnant magnetization (RM); (△) zero field-cooled magnetization (ZFCM).

Table 7. Magnetic Data of Selected A[MCr(ox)$_3$] Compounds

compound	$\chi_M T$ at 300 K (emu·K·mol^{-1})	T_c (K)	M_{sat} at 2 K (emu·mol^{-1})	remnant
DAPS[MnCr(ox)$_3$]	6.35	6	43200	zero
DAZOP[MnCr(ox)$_3$]	6.55	6	42600	medium
MHS[FeCr(ox)$_3$]	5.95	13	30400	strong up to 9 K
DAZOP[CoCr(ox)$_3$]	5.17	13	24500	strong up to 10 K
DAPS[NiCr(ox)$_3$]	3.46	14	25500	medium
DAMS[CuCr(ox)$_3$]	2.25	7	20900	strong up to 4 K

[MnCr(ox)$_3$]·CH$_3$CN is nearly zero whereas the DAMS analogue retains a significant remnant. The temperature dependence of the field-cooled, remnant, and zero field-cooled magnetizations are shown in Figure 7b. Interestingly, the magnetic data for the SHG active DAZOP analogue are closer to those of DAMS[MnCr(ox)$_3$] than of DAPS[MnCr(ox)$_3$]·CH$_3$CN.The magnetic data of a few other SHG active compounds with M = Fe, Co, Ni, Cu are shown in Table 7. In each case, the $\chi_M T$ values at 300 K are consistent with the values expected for noninteracting M^{II} and Cr^{III} ions. The compounds all order ferromagnetically at low temperature and the saturated values of the magnetization are consistent with ferromagnetic ordering. Nevertheless three points are of interest: (i) the Co and Ni compounds have much higher Curie temperatures: DAZOP-[CoCr(ox)$_3$] even displays a significantly higher T_c (13 K) than several previously reported compounds based on [CoCr(ox)$_3$]$_n^{n-}$ layers but including ferricinium or ammonium species (9−10 K);[11,15] (ii) the uprise of the $M = f(H)$ curve of the Cu, Co, and

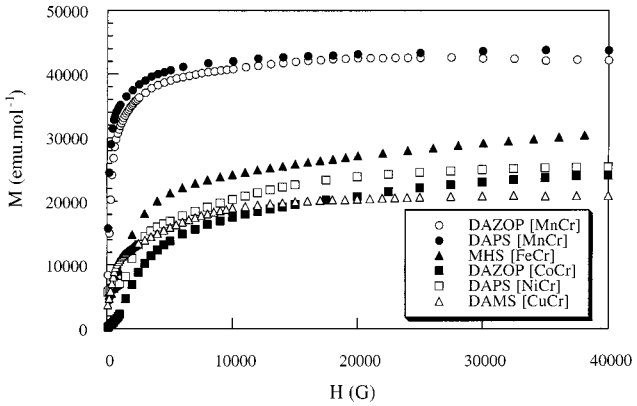

Figure 8. Field dependence of the magnetization (M) of selected A[MCr(ox)$_3$] compounds.

Ni compounds is sluggish. This effect is particularly marked with Co, where an applied field of 4 T is necessary to saturate M at 2 K (Figure 8). The study in a low field and in zero field of the Co compound also shows that the remnant remains strong up to about 10 K.

These magnetic properties deserve quite few comments, as low-temperature ferromagnetism was expected owing to the work already published on oxalates.[10−18] The sluggish character of the $M(H)$ curves at 2 K for DAZOP[CoCr(ox)$_3$] as well as the large remnant merely reflects the strong anisotropy of the electronic structure of the Co^{II} ions. The small differences between the magnetic data of DAZOP[MnCr(ox)$_3$] and DAPS-[MnCr(ox)$_3$]·CH$_3$CN (persistence of a remnant magnetization in the former) might reflect the anisotropy induced by the aligned electric dipoles of DAZOP, but they can also be due to differences in the microstructure of the two compounds.

UV−Visible Spectroscopy. The UV−visible spectra of various DAMS[MCr(ox)$_3$] compounds are compared in Figure 9a with the spectrum of the solid iodide (DAMS)I. Each spectrum shows a broad absorption band between 400 and 600 nm. No significant modification of the spectrum of the chromophore accompanies its inclusion between the oxalate layers. The DAZOP and DAPS analogues show similar features (Figure 9b), for example the absorption band of the chromophore is not significantly affected by the inclusion, irrespective of the SHG efficiency of the final compound.

Search for Structure−Property Relationships. The fundamental questions coming up at this point are evidently the following ones: (i) what can be said about the structure of the NLO active compounds and (ii) which factors determine an NLO active packing rather than a centrosymmetric, inactive one? In a recent work dealing with the intercalation of stilbazolium-shaped chromophores into the centrosymmetric layered MPS$_3$ host lattice, some of us have shown that SHG efficiency was due to the formation of *J*-aggregates of the chromophores within the interlayer space.[7] In the case of the oxalate compounds, aggregates clearly do not form, a conclusion supported by the absence of any significant change of the UV−visible spectra of the chromophores on passing from the pure to the included state.

Examination of Table 5 reveals that the NLO efficiency of the compounds depends on subtle factors: thus, DAPS and MIPS embedded in A[MCr(ox)$_3$] give NLO active arrangements when M = Fe^{II} or Co^{II}, whereas they do not when M = Mn^{II} or Ni^{II}. Another illustration of the high sensitivity of the chromophore packing upon very small chemical changes is the loss of SHG efficiency of the compounds on changing DAMS for DAES, that is changing the *N*-methyl group for an *N*-ethyl one on the

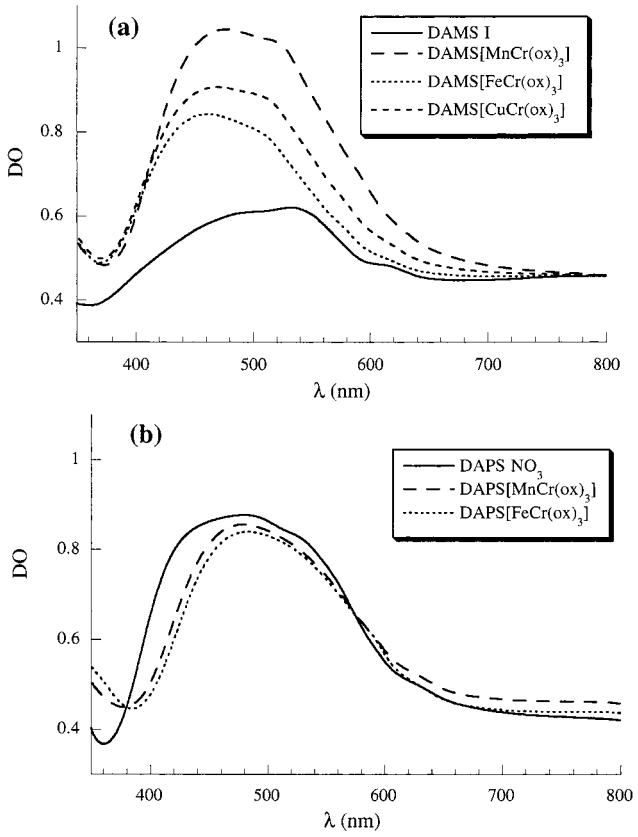

Figure 9. Electronic absorption spectra: (a) of solid DAMS iodide and of selected, DAMS[$MCr(ox)_3$] compounds (b) of DAPS nitrate and selected, DAPS[$MCr(ox)_3$] compounds.

pyridinium ring. Therefore it is probably out of reach to draw a general clear-cut conclusion regarding the factors that ultimately determine the symmetry of the chromophore packing and hence the NLO activity of the compounds.

Nevertheless a clue to this problem can be suggested if one focuses on the three compounds that display the largest efficiency (those with DAMS and DAZOP) and examine them in light of the two model structures (those with DAPS and MIPS). The three most active compounds have very short interlayer distances (8.63, 8.72, 8.77 Å). As developed below, this feature imposes severe limitations on the possible orientations of the included chromophores. Comparison of these short distances with the interlayer distance (9.92 Å) in DAPS[$MnCr(ox)_3$]·CH_3CN, where the DAPS species stand "edge on", implies that the aromatic rings of the DAZOP and DAMS chromophores in the active compounds must be considerably tilted with respect to the direction normal to the oxalate layers.

A close examination of the structure of MIPS [$MnCr(ox)_3$] allows to be more precise. In this compound, the oxalate layers are puckered and two successive layers are shifted by $a/2$ with respect to each other. This combination generates a modulation of the interlayer distance, that clearly appears in Figure 5b (viewed along the **a** axis). In those regions where the interlayer separation is large (about 9.8 Å), the aromatic rings of the MIPS chromophores are tilted by 27° with respect to the normal. In contrast, the rings are tilted by 58° in those regions where the interlayer distance is small (8.20 Å). In other terms, the local interlayer distance seems to be in close relation to the orientation of the rings. As a consequence, the interlayer distance of about 8.7 Å measured in the three active DAMS and DAZOP compounds implies that the aromatic rings of the chromophore be tilted by at least 45° with respect to the normal.

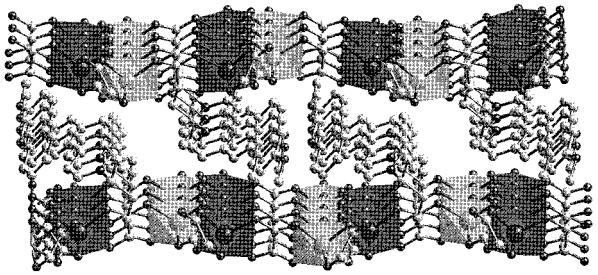

Figure 10. Perspective view of the MIPS[$MnCr(ox)_3$] structure highlighting the non-uniform occupation of the interlayer space by the MIPS chromophores. The **b** axis lies horizontally in the plane of the figure.

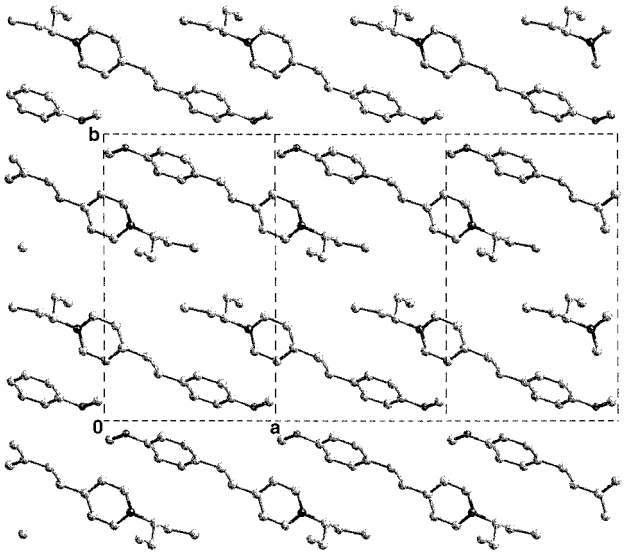

Figure 11. Top view of a MIPS layer showing that space crowding hinders possible rotations of the nearly vertical aromatic rings.

This requirement does appear as a constraint which probably precludes the chromophore dipoles to be anti-aligned. The reason is that—as shown below—dipole pairing causes nonuniform occupation of the interlayer space (alternance of dense and empty regions). As a consequence, chromophores having their dipoles paired will be located very close to each other and part of the space is unused. Consequently such arrangements will cause the interlayer distance to be quite large, because some of the aromatic rings have to remain almost perpendicular to the layers because of steric hindrance. In other words, it seems unlikely that dipole pairing can occur in a A[$MnCr(ox)_3$] compound having a basal spacing as short as 8.7 Å because under such conditions there is no space enough for the aromatic rings to be sufficiently tilted.

To give strength to the above assertions, let us consider the chromophore packing in MIPS[$MnCr(ox)_3$], where the dipoles are paired. The occurrence within the interlayer region of dense rows and empty space is evident if one considers the perspective shown in Figure 10. Looking at a top view of a MIPS layer (Figure 11), the two "nearly vertical" aromatic rings stand very close to each other (shortest distance between the rings of 3.5 Å) and they cannot be tilted much further because of steric hindrance. Hence an interlayer distance as short as 8.7 Å is not compatible with the dipole paired packing that prevails in MIPS-[$MnCr(ox)_3$]. The same considerations also hold for the structure of DAPS[$MnCr(ox)_3$]·CH_3CN. Figure 5a readily shows that the rows of DAPS chromophores that run along the **a** axis (perpendicular to the plane of the figure) are well separated, hence the puckering of the oxalate layers. The distance between

the molecular planes of adjacent DAPS molecules along the **a** axis is only 3.7 Å, and therefore an increase of their tilt angle from 0 to 45° is sterically hindered.

From the above considerations, we infer that the chromophore packing in the three most active DAMS and DAZOP compounds, which are characterized by a short interlayer distance, implies a more uniform "interlayer space filling" containing no void regions so that the chromophore rings can have free space available to allow a "flatter" orientation. Without speculating too far, the following suggestion looks reasonable. The dipolar moments of the DAMS and DAZOP chromophores in the strongly NLO active compounds are likely to be all aligned. This particular disposition of the chromophores should reduce or supress the "dimerization" between adjacent rows and therefore increase their mean separation, thus allowing the chromophores to adopt a strongly tilted orientation. This tentative model seems to be consistent with the known experimental data and will be used as a basis for Rietveld refining. Of course, the relationship discussed above between the interlayer distance and the nature of the packing can only hold when comparing compounds having nearly equal areas of the (**a**, **b**) face of the unit cell and similar chromophores. Remarkably, the (**a*b**) products of the parameters of the four compounds A $[MnCr(ox)_3]$ (A = DAMS, DAZOP, MIPS, DAPS) are all equal to 151 Å^2. The slight decrease of **a** and increase of **b** on going from the two inactive to the two active compounds are probably driven by the different relative dispositions of the chromophores.

If this model were to be confirmed, it would give a clue to the question: why do some of the compounds order with the chromophores being lined up? Part of the reason might be that the gain in energy due to a closer approach of the anionic and cationic layers (shorter interlayer distance) counterbalances the natural tendency of the strongly dipolar molecules to pair up their dipoles. An homogeneous disposition of the chromophores diminishes their mutual interaction because they are more distant on the average, but this is compensated by the increased host−guest interactions.

Conclusions

In conclusion, it turns out that the bimetallic $[MCr(ox)_3]_n^{n-}$ layers can be associated on the molecular scale to a series of hyperpolarizable chromophores to afford a new family of compounds that are NLO active and ferromagnetic. A few of these compounds, such as DAMS or DAZOP$[MnCr(ox)_3]$ are even very efficient at SHG and have strong magnetization. The connection between crystal structure and non-NLO activity is well drawn in two structures, and a model is suggested that emphasizes the importance of a short interlayer distance in the compounds which are the most active. The low Curie temperatures do not render the study of a possible interaction between magnetism and SHG easy, but the handicap can be technically overcome. In any case, the present work should be considered as a first step. Magnets with much higher Curie temperatures have already been synthesized using layered $[MFe(ox)_3]^-$ oxalatoferrates incorporating ammonium cations, and therefore it can be hoped that the inclusion of strongly hyperpolarizable chromophores in these systems could yield SHG active magnets with T_c's up to 40 K. New perspectives should also be brought by the utilization of optically pure $[Cr(ox)_3]^{3-}$ enantiomers to achieve non-centrosymmetric assemblies of chromophores.[34]

Acknowledgment. This article is dedicated to the memory of Professor Olivier Kahn.

Supporting Information Available: Net atomic charges and dipole contributions (PDF). This material is available free of charge via the Internet at http://pubs.acs.org. Crystallographic data (excluding structure factors) for the structures reported in this paper have been deposited at the Cambridge Crystallographic Data Centre and allocated the deposition numbers CCDC 134955 for DAPS$[MnCr(ox)_3]\cdot CH_3CN$ and CCDC 134956 for MIPS$[MnCr(ox)_3]$. Copies of the data can be obtained free of charge on application to The Director, CCDC, 12 Union Road, Cambridge CB2 1EZ, UK [Fax: +44(1223)-336-033. E-mail: deposit@ccdc.cam.ac.uk. World Wide Web: http://www.ccdc.cam.ac.uk].

JA0002619

(34) Andrés, R.; Gruselle, M.; Malézieux, B.; Verdaguer, M.; Vaissermann, J. *Inorg. Chem.* **1999**, *38*, 4637.